

## ENERGY RECONSTRUCTION OF ELECTROMAGNETIC SHOWERS FROM $\pi^0$ DECAYS WITH THE ICARUS T600 LIQUID ARGON TPC

A. ANKOWSKI<sup>a</sup>, M. ANTONELLO<sup>b</sup>, P.G. APRILI<sup>b</sup>, F. ARNEODO<sup>b</sup>, A. BADERTSCHER<sup>c</sup>  
 B. BAIBUSSINOV<sup>d</sup>, M. BALDO-CEOLIN<sup>d,e</sup>, G. BATTISTONI<sup>f</sup>, P. BENETTI<sup>g,h</sup>, R. BRUNETTI<sup>h†</sup>  
 A. BUENO<sup>i</sup>, E. CALLIGARICH<sup>h</sup>, M. CAMBIAGH<sup>g,h</sup>, N. CANCI<sup>b,j</sup>, F. CARONARA<sup>k,l</sup>  
 M.C. CARMONA<sup>i</sup>, F. CAVANNA<sup>b,j</sup>, P. CENNINI<sup>m</sup>, S. CENTRO<sup>d,e</sup>, A. CESANA<sup>f,n</sup>  
 K. CIEŚLIK<sup>d,o</sup>, D. CLINE<sup>p</sup>, A.G. COCCO<sup>k</sup>, A. DĄBROWSKA<sup>o</sup>, R. DOLFINI<sup>g,h</sup>, C. FARNESE<sup>d,e</sup>  
 A. FAVA<sup>d,e</sup>, A. FERRARI<sup>m</sup>, G. FIORILLO<sup>k,l</sup>, S. GALLI<sup>b,j</sup>, V. GALLO<sup>k</sup>, D. GARCIA-GAMEZ<sup>i</sup>  
 D. GIBIN<sup>d,e</sup>, A. GIGLI BERZOLARI<sup>g,h</sup>, K. GRACZYK<sup>a</sup>, A. GUGLIELMI<sup>d</sup>, J. HOLECZEK<sup>r</sup>  
 D. KIELCZEWSKA<sup>s</sup>, J. KISIEL<sup>r</sup>, T. KOZŁOWSKI<sup>t</sup>, J. ŁAGODA<sup>t</sup>, M. LANTZ<sup>f,†</sup>, J. LOZANO<sup>i</sup>  
 G. MANNOCCHI<sup>u</sup>, M. MARKIEWICZ<sup>o</sup>, A. MARTINEZ DE LA OSSA<sup>i</sup>, F. MAURI<sup>h</sup>  
 A.J. MELGAREJO<sup>i</sup>, A. MENEGOLLI<sup>h,§</sup>, G. MENG<sup>d</sup>, P. MIJAKOWSKI<sup>t</sup>, C. MONTANARI<sup>h</sup>  
 S. MURARO<sup>f</sup>, S. NAVAS<sup>i</sup>, S. OTWINOWSKI<sup>p</sup>, O. PALAMARA<sup>b</sup>, T.J. PALCZEWSKI<sup>t</sup>  
 L. PERIALE<sup>u</sup>, G. PIANO MORTARI<sup>b,j</sup>, A. PIAZZOLI<sup>g,h</sup>, P. PICCHI<sup>u</sup>, F. PIETROPAOLO<sup>d</sup>  
 W. PÓLCHLOPEK<sup>v</sup>, M. POSIADAŁA<sup>s</sup>, M. PRATA<sup>h,¶</sup>, P. PRZEWŁOCKI<sup>t</sup>, A. RAPPOLDI<sup>h</sup>  
 G.L. RASELLI<sup>h</sup>, E. RONDIO<sup>t</sup>, M. ROSSELLA<sup>h</sup>, A. RUBBIA<sup>c</sup>, C. RUBBIA<sup>b</sup>, P. SALA<sup>f</sup>  
 D. SCANNICCHIO<sup>g,h</sup>, A. SCARAMELLI<sup>f</sup>, E. SEGRETO<sup>b</sup>, F. SERGIAMPIETRI<sup>w</sup>, J. SOBCZYK<sup>a</sup>  
 D. STEFANO<sup>o</sup>, J. STEPANIAK<sup>t</sup>, R. SULEJ<sup>c</sup>, M. SZARSKA<sup>o</sup>, T. SZEGŁOWSKI<sup>r</sup>, M. SZEPTYCKA<sup>t</sup>  
 M. TERRANI<sup>f,n</sup>, F. VARANINI<sup>d</sup>, S. VENTURA<sup>d</sup>, C. VIGNOLI<sup>h</sup>, T. WĄCHAŁA<sup>o</sup>, H. WANG<sup>p</sup>  
 A. ZALEWSKA<sup>o</sup>

<sup>a</sup>Institute of Theoretical Physics, University of Wrocław, Wrocław, Poland

<sup>b</sup>INFN — Laboratori Nazionali del Gran Sasso, Assergi (AQ), Italy

<sup>c</sup>Institute for Particle Physics, ETH Höggerberg, Zürich, Switzerland

<sup>d</sup>INFN — Sezione di Padova, Padova, Italy

<sup>e</sup>Università di Padova, Padova, Italy

<sup>f</sup>INFN — Sezione di Milano, Milano, Italy

<sup>g</sup>Università di Pavia, Pavia, Italy

<sup>h</sup>INFN — Sezione di Pavia, Pavia, Italy

<sup>i</sup>Universidad de Granada and CAFPE, Granada, Spain

<sup>j</sup>Università dell'Aquila, L'Aquila, Italy

<sup>k</sup>INFN — Sezione di Napoli, Napoli, Italy

<sup>l</sup>Università Federico II di Napoli, Napoli, Italy

<sup>m</sup>CERN, Geneva, Switzerland

<sup>n</sup>CESNEF — Politecnico di Milano, Milano, Italy

<sup>o</sup>H. Niewodniczański Institute of Nuclear Physics PAN, Kraków, Poland

<sup>p</sup>UCLA — University of California, Los Angeles, California, USA

<sup>q</sup>Institute of Physics, University of Silesia, Katowice, Poland

<sup>r</sup>Institute of Experimental Physics, University of Warsaw, Warsaw, Poland

<sup>t</sup>A. Sołtan Institute for Nuclear Studies, Warsaw, Poland

<sup>u</sup>INFN — Laboratori Nazionali di Frascati, Frascati (Roma), Italy

<sup>v</sup>AGH University of Science and Technology, Kraków, Poland

<sup>w</sup>INFN — Sezione di Pisa, Pisa, Italy

<sup>x</sup>Institute of Radioelectronics, Warsaw University of Technology, Warsaw, Poland

*(Received July 24, 2009; final version received November 16, 2009)*

<sup>†</sup> Now at INFN — Sezione di Torino, Torino, Italy.

<sup>‡</sup> Now at Chalmers University, Sweden.

<sup>§</sup> Corresponding author: [alessandro.menegolli@pv.infn.it](mailto:alessandro.menegolli@pv.infn.it)

<sup>¶</sup> Now at LENA, Università di Pavia, Italy.

We discuss the ICARUS T600 detector capabilities in electromagnetic shower reconstruction through the analysis of a sample of 212 events, coming from the 2001 Pavia surface test run, of hadronic interactions leading to the production of  $\pi^0$  mesons. Methods of shower energy and shower direction measurements were developed and the invariant mass of the photon pairs was reconstructed. The  $(\gamma, \gamma)$  invariant mass was found to be consistent with the value of the  $\pi^0$  mass. The resolution of the reconstructed  $\pi^0$  mass was found to be equal to 27.3%. An improved analysis, carried out in order to clean the full event sample from the events measured in the crowded environment, mostly due to the trigger conditions, gave a  $\pi^0$  mass resolution of 16.1%, significantly better than the one evaluated for the full event sample. The trigger requirement of the coincidence of at least four photo-multiplier signals favored the selection of events with a strong pile up of cosmic ray tracks and interactions. Hence a number of candidate  $\pi^0$  events were heavily contaminated by other tracks and had to be rejected. Monte Carlo simulations of events with  $\pi^0$  production in hadronic and neutrino interactions confirmed the validity of the shower energy and shower direction reconstruction methods applied to the real data.

PACS numbers: 13.20.Cz, 29.40.Vj

## 1. Introduction

The Liquid Argon (LAr) Time Projection Chamber (TPC) is an option for the next generation of very large mass neutrino detectors. The LAr TPC was proposed by Rubbia [1] in 1977 and, after many years of extensive R&D studies the T600 ICARUS detector [2] has been constructed. The read-out of ionization electrons traveling in a uniform electric field provides the spacial reconstruction of an event and allows for calorimetric measurement of the energy release. In year 2001, the T600 ICARUS detector was extensively tested in Pavia (Italy), with an exposure to cosmic rays at the Earth surface. During over 100 days of continuous data taking, about 30000 cosmic ray events have been collected. In a series of papers the ICARUS Collaboration presented the following results from the T600 detector test run: observation of long ionizing tracks [3], LAr purity [4], electron recombination in LAr [5] and measurement of through-going particle momentum by means of multiple scattering [6]. The analysis of the sample of stopping  $\mu$  events led to the measurement of the  $\mu$  decay spectrum, and allowed to determine the energy resolution of the T600 ICARUS detector for the measurement of electrons with energy lower than about 50 MeV [7].

The ICARUS T600 detector is at present in the final phases of re-assembling in the underground Hall B at INFN Laboratori Nazionali del Gran Sasso (LNGS), Italy, and its commissioning is foreseen to start within the end of year 2009.

In this paper we discuss the ICARUS detector capabilities in electromagnetic shower reconstruction through the analysis of a sample of events with hadronic interactions leading to the production of  $\pi^0$  mesons. The decay of a particle with known mass gives a good test for the energy calibration. Another motivation for such studies is the following: in order to distinguish  $\nu_e$  charge current (CC) interaction

$$\nu_e + n \rightarrow e^- + p, \quad (1)$$

from the  $\nu_\mu$  neutral current (NC) interaction

$$\nu_\mu + n \rightarrow \nu_\mu + \pi^0 + \text{hadrons}, \quad (2)$$

a very good detector capability to separate electrons and pions is required. The  $\pi^0$  decays in about 98.8% into two photons. The Dalitz decays, leading to the production of one photon and electron–positron pair, compose about 1.2%. Both photons and electrons may create electromagnetic showers and therefore lead to the similar event topology for both NC and CC interactions.

The paper is organized as follows. The ICARUS T600 detector set-up is briefly described in Section 2. Section 3 concerns the search and the selection of cosmic ray hadronic interactions in T600 detector with the production of the  $\pi^0$  meson. In Section 4 the methods used for the measurement of the energy released in LAr by the two electromagnetic showers coming from  $\pi^0 \rightarrow \gamma \gamma$  decay and for the reconstruction of  $\pi^0$  mass are illustrated. The analysis of the selected event sample from real data is presented in Section 5. In Section 6 the precision in the measurement of the electromagnetic shower energy deposition in LAr is evaluated in the condition of the test experiment through a simulation of electrons and photons showering inside T600 detector. In Section 7 the Monte Carlo simulations of  $\pi^0$  in ICARUS T600, used to validate the reconstruction routines for electromagnetic showers, are shown. In Section 8 the same method of event reconstruction used for the real data is applied to Monte Carlo simulated muon neutrino interactions with  $\pi^0$  production. The possible mixing of such events with the electron neutrino CC interaction is discussed. The work is summarized and concluded in Section 9.

## 2. Experimental set-up

The T600 ICARUS detector is composed of two identical adjacent “T300” half-modules filled with Liquid Argon. Two Time Projection Chambers (TPCs) with common cathode placed in the middle, the electric field shaping system, LAr purity monitors and photo-multiplier tubes (PMTs) are enclosed in each half-module. The external thermal insulation, together with a Liquid Nitrogen circuit, allows to stabilize the LAr temperature. The

required LAr purity is achieved by a purification system. Each T300 half-module has the following internal dimensions: 3.6 m (width), 3.9 m (height) and 19.9 m (length). Along the longest side walls (left and right) of each half-module, three parallel planes (two *Induction* planes and one *Collection* plane) of anode wires are placed. They are parallel to the cathode and form two TPCs. They are oriented at  $60^\circ$  with respect to each other, 3 mm apart, with wire pitch of 3 mm. The total number of wires in the T600 detector is 53248, whereas the volume of LAr in the instrumented part of the detector is  $340.3 \text{ m}^3$  (476.5 tons). The ionization electrons, forced by a uniform electric field of 500 V/cm perpendicular to the cathode, drift toward the anode wires inducing a signal on those which they pass by. The appropriate voltage biasing causes non-destructive signal to be induced first on two Induction wire planes, whereas the ionization electrons charge is finally collected in the Collection wire plane. By combining the information from two-dimensional projections, provided by each pair of wire planes, with the position along the drift time, it is possible to obtain a three-dimensional reconstruction of an event. The zero time  $t_0$  of an event is defined by the PMT detection of LAr scintillation light. The position along the drift time is given with respect to  $t_0$ .

Several triggers have been applied during the T600 ICARUS detector test run. An external trigger system made of plastic scintillators was used for detection of muon tracks. An independent trigger system was based on photomultipliers, which detect scintillation light produced during interaction of charged particles with LAr. Most of the  $\pi^0$  candidates used in this analysis were found in the data collected with this internal trigger. The detailed description of the T600 ICARUS detector design, construction, and performance is given in [2], where the conditions of the technical run and the event off-line reconstruction procedure are discussed as well.

### 3. Data selection

Interactions in LAr producing  $\pi^0$ s decaying into photons have been selected through a visual scanning for events with at least two showers pointing to the interaction vertex: Fig. 1 shows an example of an ICARUS T600 full view event, with a  $\pi^0$  candidate that was selected during the scanning phase. Most of the selected interactions are initiated by hadrons, hence we also use the term “hadronic interactions”. Altogether, about 7500 images have been scanned. The majority of the events were collected with triggers based on signals from photomultipliers, rich in hadronic interactions.

It has to be stressed that the T600 ICARUS test run internal trigger based on photomultipliers was aimed at air showers, so that many events were not measurable because of their complexity due to a crowded environment. The surface exposure has, in fact, as a result that a number of

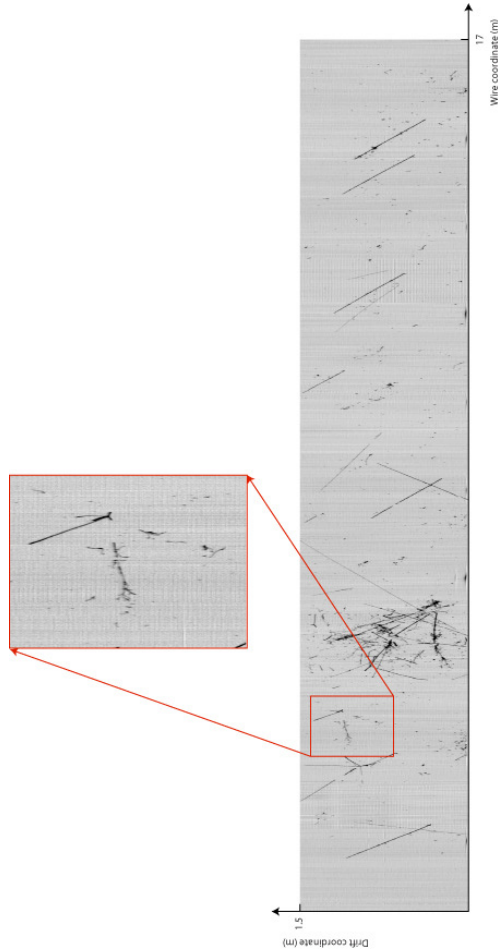


Fig. 1. Example of an ICARUS T600 full view event (Run 939 Event 130). The scale of the image does not match the real one, that is 17 m (wire coordinate, vertical axis)  $\times$  1.5 m (drift coordinate, horizontal axis). On the right side, close to the center of the image, a large hadronic interaction leading to the production of a number of secondaries is visible. Along all the image m.i.p. tracks can be seen. A zoomed view of an hadronic interaction leading to  $\pi^0$  production and subsequent decay in two photons is shown.

candidate  $\pi^0$  events can lie in zones of the detector of strong pile up of cosmic ray events, which can partially overlap the electromagnetic showers of the photons of the  $\pi^0$  decay. This affects either the capability of the visual scanning in disentangling the good events from an environment populated by many through-going particles or the precision in the shower energy reconstruction for selected events with partial overlap with cosmic ray events.

The following scanning rules were adopted for the pre-selection of hadronic interactions with  $\pi^0$  production:

- At least two, well separated electromagnetic showers originated by photons pointing to the interaction vertex are demanded. Shower vertices and directions are defined by the initial electron–positron pairs, so that it is often easy to decide if they are pointing to the interaction vertex. The showers, as well as the interaction vertex, must be clearly visible in at least two views.
- Knowledge of the event zero time ( $t_0$ ) is mandatory in order to determine the interaction vertex and the shower spatial positions in the chamber, as well as to apply proper corrections to the collected signals for the charge attenuation due to the finite electron lifetime in argon, associated to the electron attachment process to electro-negative impurities.

A unique  $t_0$  determination is possible in the following cases: (1) at least one track (but not showers) from the interaction is crossing the anode wires ( $t_0 = 0 \mu\text{s}$  for crossing points); (2) at least one track (but not showers) is crossing the cathode plane ( $t_0 = 962 \mu\text{s}$  for crossing points); (3) an unique association between the interaction and the PMT induces signals on Collection wires (Fig. 2).

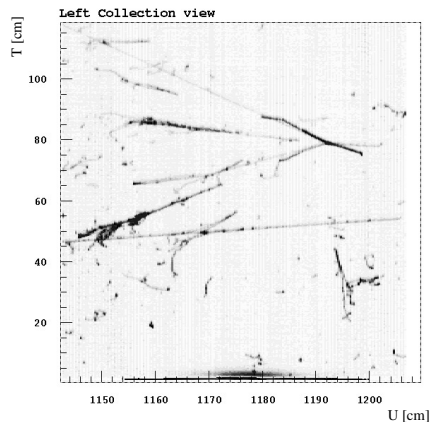


Fig. 2. An example of a real event in which the  $t_0$  is uniquely determined from PMT induced signal on Collection wires, visible at the drift coordinate  $T \sim 0$  cm as an ionization strip along the horizontal  $U$  wire coordinate (Run 700 Event 58).

- Interactions with neutral pion candidates are rejected when ionization due to other tracks and interactions in their neighborhood is so high that it seriously influences the shower energy determination.

Every candidate event was analyzed independently by (at least) two groups from different laboratories in the Collaboration. After all these requirements altogether 212 hadronic interactions with at least one candidate  $\pi^0$  meson were collected for further analysis. As said before, the crowded environment of ICARUS T600 test run data reduced the usable data sample substantially: examples of accepted and rejected events with neutral pion candidates are shown in Fig. 3 and in Fig. 4, respectively.

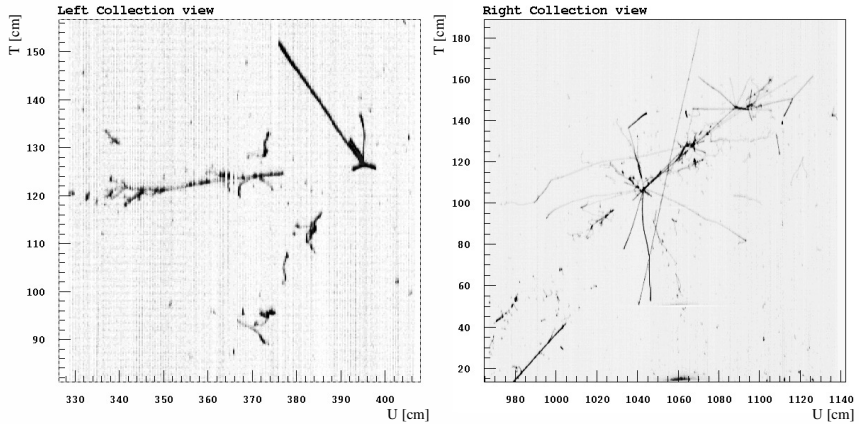


Fig. 3. Examples of real events from the final data sample: (left plot)  $\pi^0$  candidate (Run 939 Event 130); (right plot) a multi-shower event (Run 939 Event 190).

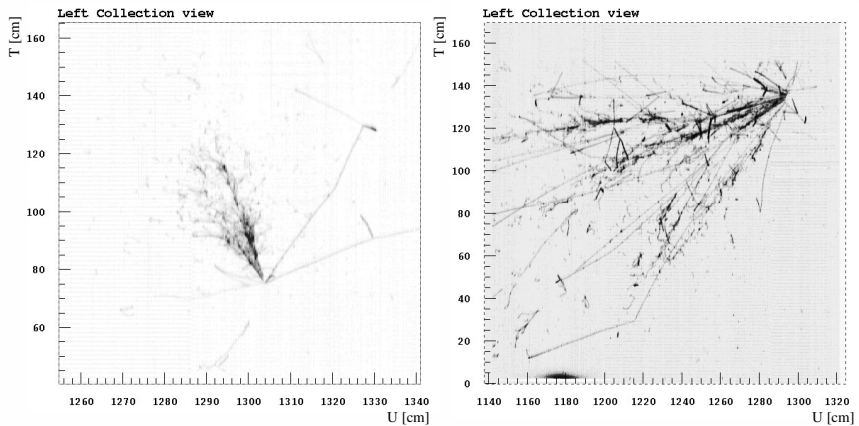


Fig. 4. Examples of real candidates not included in the final data sample: (left plot)  $\pi^0$  neutral candidate with overlapping photon showers (Run 975 Event 65); (right plot) candidate event in a crowded environment (Run 710 Event 29).

#### 4. Data reconstruction

The invariant mass  $M$  of a particle decaying into two photons is given by

$$M = \sqrt{2 E_1 E_2 (1 - \cos \theta_{12})}, \quad (3)$$

where  $E_1$  and  $E_2$  are the energies of the two photons and  $\theta_{12}$  is the angle in between. In our case, the goal was to measure the energies of two electromagnetic showers coming from the photons and to reconstruct the photon directions.

In Fig. 5, one of the 212 selected events is shown: in both Collection and Induction views an hadronic interaction vertex and the two shower starting points are visible. The drift position coordinate  $T$ , where  $T(\text{cm}) = \text{drift time (s)} \times \text{electron drift velocity (cm/s)}$ , is common for the two 2D projections of the events, while the  $U$  (cm) and  $V$  (cm) wire coordinates indicate the wire position in Collection and Induction views, respectively. The  $U$ ,  $V$  and  $T$  coordinates of the interaction vertex and those of the e.m. shower starting points are used for the three dimensional reconstruction of the photon direction, hence of the angle  $\theta_{12}$  between the two photons of the  $\pi^0$  decay.

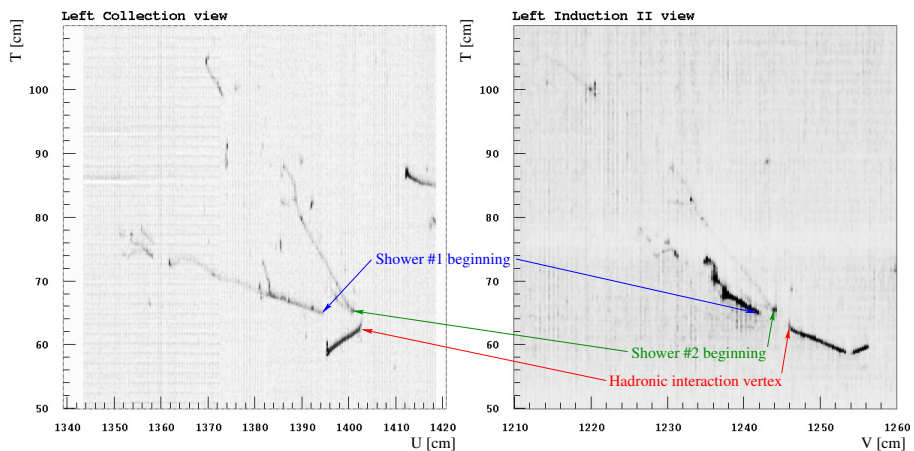


Fig. 5. Example of a real selected candidate  $\pi^0 \rightarrow \gamma \gamma$  event (Run 712 event 7). Hadronic interaction vertex and e.m. shower starting points are indicated in both Collection and Induction views.

The basic step for the calorimetric reconstruction of electromagnetic showers is the hit finding and reconstruction procedure. We define *hit* as the portion of particle track whose energy is read by a given wire. The



hit search and reconstruction is performed on the raw signal of the Collection wire plane following the standard procedure for ICARUS data analysis described in [2]. After hit reconstruction, the following parameters are available for each hit: its wire-drift position  $U$  and  $T$  and its area ( $\text{ADC} \times \mu\text{s}$ ).

A dedicated HIGZ-based Graphical User Interface visualization tool allows to select directly the region with the hits belonging to a shower, by building a polygonal line around the shower directly on the Collection view by means of interactive calls of HIGZ ambient. Then hit finding routine is applied within the bounds defined by the polygonal line (see Fig. 6). It has to be noticed that the definition of the area surrounding the shower is left to the user choice, so that small variations of the reconstructed energy can be found between measurements done by different users. This happens especially in the case the two photons of the  $\pi^0$  decay are emitted at small angle, so it can be difficult to decide whether an energy deposition belong to the first shower or to the second one.

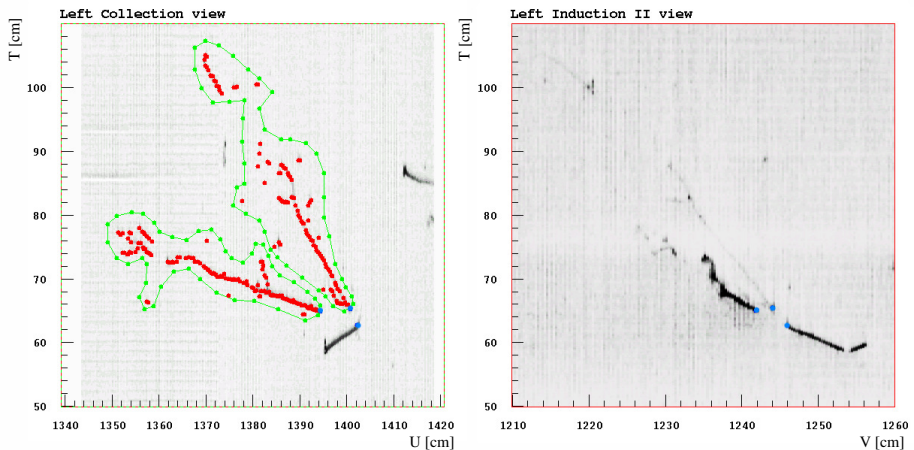


Fig. 6. Example of the application of the routines that allow to select the hits belonging to an e.m. shower: the polygonal lines are built by the user. Reconstructed hits inside the areas defined by the polygonal lines are marked with dots (red) (Run 712 event 7).

Once all hits belonging to a shower are found, the overall shower energy  $E_s$  is computed by summing all energies  $E$  of the hits inside the shower area:

$$E \text{ (MeV)} = \frac{1}{\varepsilon} \frac{CW}{R} \frac{1}{A} Q, \quad (4)$$

where:  $C = (152 \pm 2) \times 10^{-4}$  fC/(ADC  $\times$   $\mu\text{s}$ ) is the calibration factor [4];  $W = 23.6_{-0.3}^{+0.5}$  eV is the average energy needed for the creation of an electron–

ion pair [8];  $R = 0.640 \pm 0.013$  is the electron–ion recombination factor [7];  $A = e^{-\frac{t-t_0}{\tau_e}}$  is the drift electron lifetime attenuation factor:  $t$  is the hit drift time coordinate and  $t_0$  is the event zero-time.  $\tau_e$  is the actual electron lifetime in LAr, that varies run by run [4]. For example, in  $\pi^0$  data samples used here the electron lifetime changes from 0.93 ms to 1.65 ms (mean value = 1.43 ms), and the typical value of the drift time is about one millisecond. Its value as a function of the acquisition date was monitored during the T600 data taking [9], with relative errors at the level of 5%; finally,  $Q$  is the hit area. Then, the shower energy  $E_s$  has been corrected for the inefficiency of the reconstruction method. It was done using showers and electrons in the range 50–5000 MeV in ICARUS T600 from the Monte Carlo simulations (for details, see Sec. 6.) The efficiency factor  $\varepsilon$  was calculated as the ratio between measured and generated shower energy. The shower energy of the real data, after some fiducial volume cuts, was corrected by multiplying it by the factor  $1/\varepsilon$ . It has to be noticed that the correction for the reconstruction efficiency in Eq. (4) depends on the attenuation factor  $A = e^{-(t-t_0)/\tau_e}$  coming from the drift electron finite lifetime of the Monte Carlo generated events, so that the  $\varepsilon$  value changes shower by shower, ranging from  $\varepsilon = 0.69 \pm 0.03$  ( $A = 0.5$ ) to  $\varepsilon = 0.83 \pm 0.04$  ( $A = 1$ ) (see Fig. 11). The error on the shower energy is then evaluated from the propagation of all contributions in Eq. (4).

The angle  $\theta_{12}$  between photons is then evaluated from the spatial coordinates of hadronic interaction vertex and of starting points of the showers as explained above.

## 5. Results

### 5.1. $(\gamma, \gamma)$ invariant mass

Most of the 212 events forming the sample were measured in several laboratories. The difficult condition of data analysis due to the presence of a crowded environment sometimes has as a result that the same event measured in different laboratories produces different values in vertex coordinate and shower energy determination. As explained above, the somehow arbitrary choice of the user to build the polygonal line surrounding the e.m. photon shower of the  $\pi^0$  decay could in principle introduce some systematics in the  $(\gamma, \gamma)$  invariant mass distributions coming from different laboratories. Fig. 7 shows the  $(\gamma, \gamma)$  invariant mass distribution of three sub-samples of events, each provided by a different laboratory involved in the data analysis. It appears that on average no systematic differences between measurements carried out in different laboratories are present. At this stage of the analysis, the  $\varepsilon$  parameter taking into account the shower energy reconstruction efficiency, see Eq. (4), has not been considered yet, hence the mass values for some of the  $\pi^0$ s are underestimated with respect to the nominal ones.

As a remark, it has to be noticed that in LNGS underground condition the events will be very clean, so that each  $\pi^0$  decay event will be measured just once unambiguously. The event sample for the following analysis was then built by taking just one measurement per event chosen randomly from the available ones in the case of events measured by more than one laboratory, then adding to the sample all the other events measured just once.

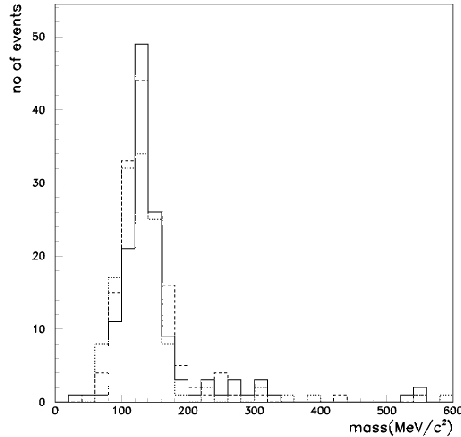


Fig. 7.  $(\gamma, \gamma)$  Real event invariant mass distributions (solid, dotted and dashed lines) of three different laboratories involved in the data analysis.

A preliminary consistency check was performed on this event sample: the distribution of distances of the shower starting points from the corresponding interaction vertex is related to the radiation length  $X_0$  in LAr,  $X_0 = 0.14$  m [10]. This is shown in Fig. 8. The value of the mean distance obtained from a fit with an exponential function is:

$$X_\gamma = (0.174 \pm 0.008) \text{ m}, \quad (5)$$

that is in agreement with the expected length for photons  $X_\gamma = \frac{9}{7} X_0 = 0.18$  m for LAr.

A fiducial volume cut was then applied by requiring that at least the first three radiation lengths of both showers were fully contained in the chamber. This reduced the event number to 164, of which 126 were two-shower and 38 were multi-shower events; the final number of  $\pi^0$  candidates in the selected event sample was then found to be equal to 196. At this stage of analysis the efficiency factor  $\varepsilon$  was applied in shower energy calculation.

The invariant  $(\gamma, \gamma)$  mass distribution of this 196  $\pi^0$  candidate sample is shown in Fig. 9, as well as the  $\pi^0$  energy distribution. The correct mass combinations of multi-shower events were disentangled after the minimization of the parameter:

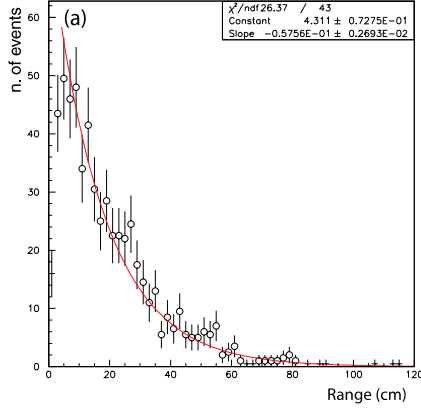


Fig. 8. Distribution of the distances between shower starting point and interaction vertex for LAr radiation length evaluation.

$$\chi^2 = \sum_{i=1}^n \left( \frac{m_{\pi^0} - m_i}{\sigma_i} \right)^2 \quad (6)$$

evaluated for all the possible combinations of showers. ( $m_{\pi^0} = 135 \text{ MeV}/c^2$  [10]). Here,  $n$  is the maximum number of  $\pi^0$ s allowed (1 for a three shower event, 2 for a four and five shower event, 3 for a 6 shower event). The average mass given by a Gaussian fit is:

$$m_{\gamma\gamma} = 134.4 \pm 3.0 \text{ MeV}/c^2. \quad (7)$$

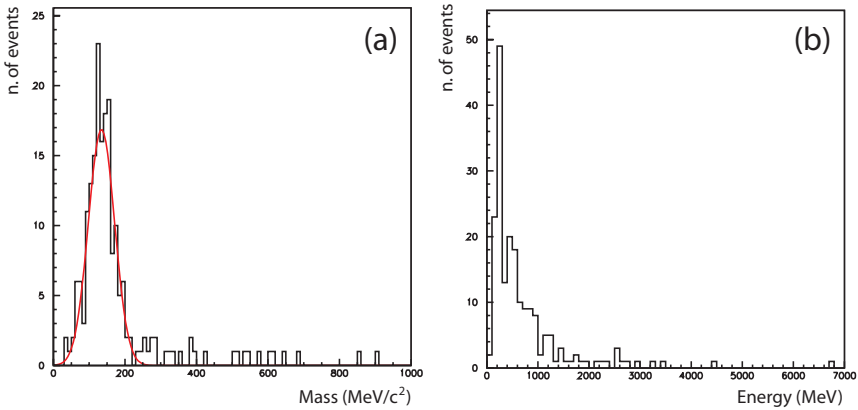


Fig. 9.  $(\gamma, \gamma)$  invariant mass (a) and energy (b) distributions for the sample of 196 real  $\pi^0$  candidates. The average mass is  $m_{\gamma\gamma} = 134.4 \pm 3.0 \text{ MeV}/c^2$  ( $\sigma = 36.7 \pm 3.4 \text{ MeV}/c^2$ ). The mean value of the  $\pi^0$  energy is  $E = 707.7 \text{ MeV}$ .

The evaluation of all systematic contributions to the error on the  $\pi^0$  mass (see Sec. 4) introduces an additional contribution to the mass error of 7.1% (9.5 MeV/ $c^2$ ). The RMS uncertainty of the reconstructed mass was found to be equal to  $\sigma = 36.7 \pm 3.4$  MeV/ $c^2$  (27.3%). Thus the result, in agreement with the  $\pi^0$  mass, demonstrates that our mass reconstruction method is reliable.

### 5.2. Crowded environment suppression

Although on average the measurements done in different laboratories are in agreement, see Fig. 7, nonetheless for this particular analysis of events collected on surface by exposure by cosmic rays it has been chosen to improve the results by cleaning the 212 event sample from the events measured in a crowded environment. To do so, further rejection cuts were related to the consistency of the two independent measurements performed in different laboratories, see Section 3. The purpose of this refined analysis is to show that in an environment more similar to the one expected in the underground laboratory the  $\pi^0$  mass distribution has to be narrower than the one found for the full sample.

The interaction vertex and shower starting point coordinates are then considered to be in agreement if the absolute value of the differences between two independent measurements of all three coordinates is smaller than five times the width of the distribution of such differences. The distributions of the differences  $dx$ ,  $dy$ ,  $dz$  were highly non-Gaussian, with a narrow central maximum and rather flat long tails. This is probably due to the fact that either almost the same hit was measured or the difference was due to the different recognition of the first point of the shower. The “sigma” was calculated for the central peaks. For such distributions the three sigma cut does not correspond to a well defined probability value. We decided to release the cut from three to five sigma not to reject all the events with ambiguous origin.

Then, if the relative difference  $(E_1 - E_2) / \frac{(E_1 + E_2)}{2}$  between measurements of the shower energies is smaller than 50%, then the measurements are considered to be in agreement, so that only these are used to built the final  $\pi^0$  mass distribution. The values used for these cuts largely suppress the  $\pi^0$  decay events belonging to a crowded environment while keeping a relatively high statistics for the following analysis. For events which passed these tests the average values of the measured positions and energies were calculated and used for  $\pi^0$  mass determination.

The sample which passed these selection criteria was then composed of 89 events with at least one  $\pi^0$  candidate; 72 were two-shower and 17 were multi-shower events. As done for the global data sample, the correct mass combinations of multi-shower events were disentangled after the minimiza-

tion of the  $\chi^2$  parameter, see Eq. (6), evaluated for all the possible combinations of showers. After this procedure, a final sample of 97  $\pi^0$  candidates was available for the analysis.

The  $(\gamma, \gamma)$  invariant mass distribution for the final sample of 97  $\pi^0$  candidates is shown in Fig. 10(a) together with the total  $\pi^0$  energy in Fig. 10(b). The average mass given by a Gaussian fit was:

$$m_{\gamma\gamma} = 139.9 \pm 2.8 \text{ MeV}/c^2, \quad (8)$$

with a systematic contribution of 9.9  $\text{MeV}/c^2$ . The  $\pi^0$  mass resolution is now equal to 16.1% ( $\sigma = 22.6 \pm 2.9 \text{ MeV}/c^2$ ), that is 11.2% less than the one evaluated for the sample without consistency cuts. This demonstrates that in the particular case of the ICARUS T600 Earth surface data, a refined analysis was necessary in order to take into account the strong contribution of the crowded environment surrounding some of the  $\pi^0$  production and decay events. These crowded events are very difficult to analyze and bring to major differences between measurements carried out in different laboratories.

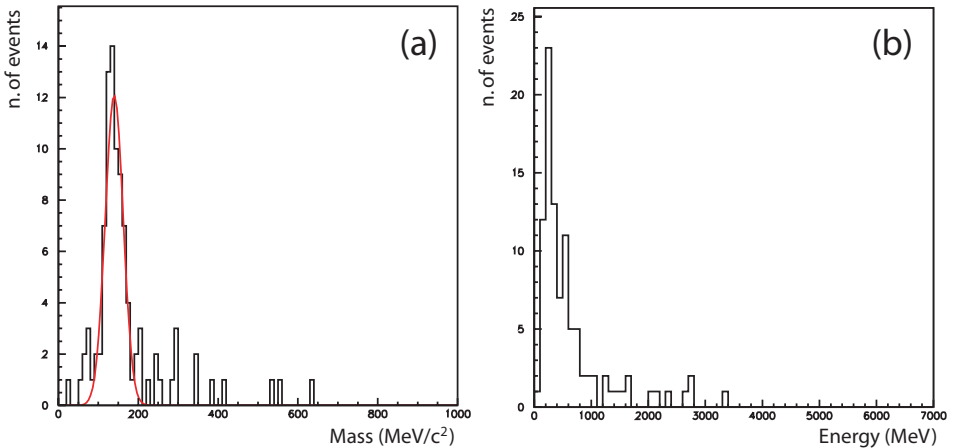


Fig. 10.  $(\gamma, \gamma)$  invariant mass (a) and energy (b) distributions for the final sample of 97 real  $\pi^0$  candidates obtained after crowded environment suppression. The average mass is  $m_{\gamma\gamma} = 139.9 \pm 2.8 \text{ MeV}/c^2$  ( $\sigma = 22.6 \pm 2.9 \text{ MeV}/c^2$ ). The mean value of the  $\pi^0$  energy is  $E = 641.8 \text{ MeV}$ .

## 6. Energy resolution for electromagnetic showers

In this section an analysis of the energy resolution for electromagnetic showers in the energy range  $50 \div 5000 \text{ MeV}$  is presented. The energy of simulated electrons and photons inside the ICARUS T600 detector was

reconstructed with the same tools used for the  $\pi^0$  events. The simulation was performed using the FLUKA [11] program for the samples of electrons and photons generated at six different energies with different orientation in the detector. The measured average energies appeared to be shifted with respect to the true energies defined at the generation. To obtain an agreement between generated and reconstructed energies, the shower energy reconstruction efficiency (*i.e.* the ratio between measured and generated shower energy)  $\varepsilon$  has to be taken into account. The inefficiency can be due to misidentification of the hits by the hit finding algorithms, as well as to the loss of the tail of the reconstructed tracks, whose energy deposition can become lower than the intrinsic wire background noise, especially in the case of low values of the electron lifetime  $\tau_e$ : in this case the drift electron finite lifetime factor  $A = e^{-\frac{t-t_0}{\tau_e}}$  is crucial. In Fig. 11 the reconstruction efficiency  $\varepsilon$  as a function of  $A$  is shown, measured for a sample of Monte Carlo events at several values of  $\tau_e$ : it is found that  $\varepsilon$  rises with  $A$ , and that it is well fitted with a fourth degree polynomial. Despite the arbitrariness of the choice of this particular function for the fit of  $\varepsilon$  *versus*  $A$ , it was found that choosing other types of curves for the fit did not introduce systematics in the value of  $\varepsilon$ , the fluctuations of which remain always well below the 1% in the region  $A = (0.5 \div 1.0)$  where the real data lie.

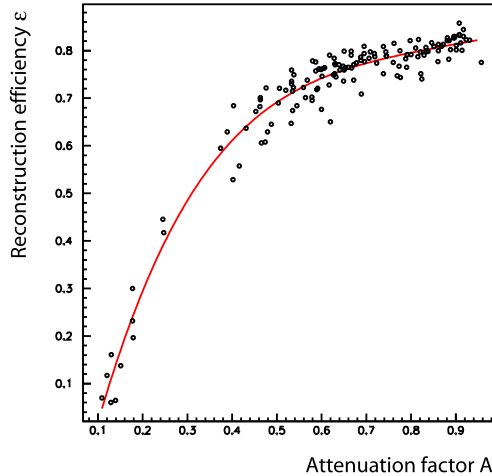


Fig. 11. Reconstruction efficiency  $\varepsilon$  as a function of drift electron finite lifetime factor  $A$ : data have been fitted with a fourth degree polynomial.

Depending on the values of this attenuation factor measured in the real data,  $\varepsilon$  was found to range from  $0.69 \pm 0.03$  ( $A = 0.5$ ) to  $0.83 \pm 0.04$  ( $A = 1$ ). Moreover, in the range of e.m. shower energy analyzed, no dependence of  $\varepsilon$  from the shower energy, the attenuation factor being the same, was found.

The effect of the  $\varepsilon$  parameter taking into account the shower energy reconstruction efficiency is shown in Fig. 12, where the dependence of the reconstructed  $\pi^0$  mass from the distance between the main hadronic interaction vertex and the wires is shown (sample of the 196  $\pi^0$  candidates). When the  $\varepsilon$  efficiency is not taken into account (dark grey (red) dots), an effect of underestimation of the mass, especially near the cathode ( $y = 150$  cm), is evident. After the shower energy correction (light grey (green) dots), this effect is much smaller and, as expected, the correction is larger for events far from wires ( $y \gtrsim 60$  cm). This effect can be seen in a more quantitative way by giving the values of the  $\chi^2$ s from the fit of the two distributions with a flat line. The value of  $\chi^2/\text{ndf}$  after the shower energy correction ( $\chi^2/\text{ndf} = 1.55/4$ ) is significantly smaller than the one without correction ( $\chi^2/\text{ndf} = 5.52/4$ ), demonstrating that after the correction the mass distribution is almost flat.

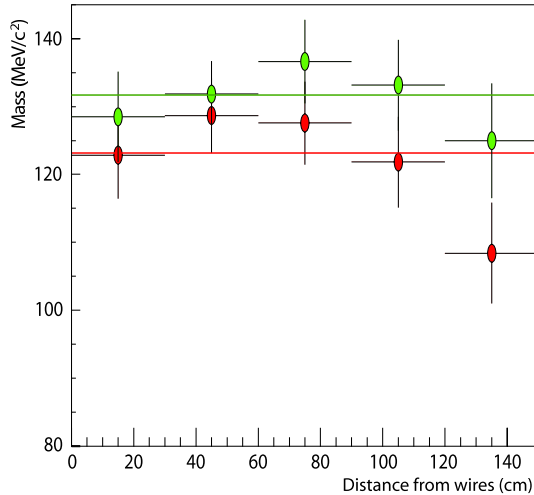


Fig. 12. Dependence of the reconstructed  $\pi^0$  mass from the distance between the main hadronic interaction vertex and the wires with (light grey (green) dots) and without (dark grey (red) dots) the correction for the  $\varepsilon$  reconstruction efficiency parameter. The red (green) straight represents the result of a fit of the red (green) dots with a flat line.

The energy resolution at fixed energies is given by the RMS of the measurements. The following formula was fitted to the measured points corresponding to simulated showers:

$$\frac{\Delta E}{E} = \frac{P1}{\sqrt{E}} + P2, \quad (9)$$



where  $P1$  and  $P2$  are the free parameters of the fit. The first part of the formula represents the typical electromagnetic calorimeter behavior. The introduction of  $P2$  parameter improves the fit quality. Its presence can be due to the fact that the amount of low energy signals at the end of the showering process grows with the initial energy. These signals can be mixed with the overall background when the hits belonging to the shower are selected. Fig. 13 illustrates the resulting energy resolution of the T600 ICARUS detector in the reconstruction of the electromagnetic showers.

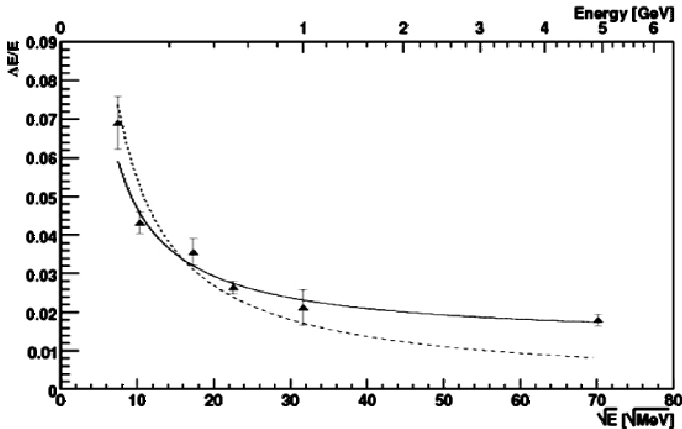


Fig. 13.  $\frac{\Delta E}{E}$  as a function of  $\sqrt{E}$  for simulated electromagnetic showers. Dashed line — fit to Eq. (9) ( $P2 = 0$  assumed), solid line — fit to Eq. (9).

The best fit with the formula of Eq. (9) was obtained for the following parameter values:  $P1 = (0.33 \pm 0.03) \sqrt{\text{MeV}}$  and  $P2 = 0.012 \pm 0.002$ . The energy resolution in LAr detector was previously studied on a base of a sample of MC generated low energy electrons ( $E < 50$  MeV) [7]: the best fit was obtained for  $P1 = (0.11 \pm 0.01) \sqrt{\text{MeV}}$  and  $P2 = 0.025 \pm 0.03$ . However, in that case  $P1$  and  $P2$  were correlated because of the small energy interval involved. The worse resolution for the high energy electromagnetic showers can be explained by larger fluctuations of integrated background because of the larger area covered by the shower as well as to the hits overlapping in the regions of large density of electron tracks. Moreover, in the case of a high energy shower it is not obvious which surrounding signals still belong to the shower. The energy resolution has been obtained for the specific method of energy reconstruction based on calorimetric information from Collection view only.

As a check of the reliability of the energy reconstruction method, the distribution of the so-called “pulls”:  $pull(m_{\pi^0}) = \frac{(m_{\gamma\gamma} - m_{\pi^0})}{\sigma(m_{\gamma\gamma})}$  was calculated for the real data, using Eq. (9) to calculate the error  $\sigma(m_{\gamma\gamma})$  as a function of  $\sigma(E_\gamma)$ . The RMS of the distribution was found to be equal to one within errors, confirming the validity of the formula obtained on the base of the measurements of the photon showers.

## 7. Monte Carlo simulation of $\pi^0$ production from hadronic interactions

Monte Carlo simulations of three different samples of  $\pi^0$ s with different kinematic and event environment conditions were carried out. The events have been generated using the FLUKA full simulation of T600 detector. They allowed to confirm the validity of the  $\pi^0$  mass reconstruction tools in environments similar to the one coming from real data. The three generated  $\pi^0$  samples were:

- (1)  $\pi^0$  decays at rest; the invariant mass is reconstructed as a sum of the photon energies since the relative angle is exactly equal to  $180^\circ$ . Only errors on the photon energies contribute to the mass resolution.
- (2)  $\Sigma^+ \rightarrow \pi^0 + p$  with subsequent  $\pi^0$  decay; the pion from the two body decay at rest has fixed momentum of 189 MeV/c and the vertex of  $\pi^0$  decay is precisely determined by the position of the low energy proton from  $\Sigma^+$  decay. Shower vertices are also well determined because no tracks overlap and affect their recognition.
- (3)  $\pi^0$  decays observed in interactions of  $\pi^-$  mesons with argon nuclei at 2 GeV incident energy. The events resemble most our real events, corresponding to hadronic interaction.

Examples of each class of these events are shown in Fig. 14. The  $(\gamma, \gamma)$  invariant mass distribution for the three measured Monte Carlo samples is shown in Fig. 15(a), 15(b) and 15(c). It can be seen that the position of the  $m_{\gamma\gamma}$  peak is consistent with the pion mass for all three generated  $\pi^0$  samples.

The RMS of the invariant mass distributions presented in Fig. 15 are equal to  $(7.4 \pm 1.3)$  MeV,  $(10.7 \pm 4.8)$  MeV and  $(25.8 \pm 4.7)$  MeV. The evident increase in RMS is mainly due to the event crowded environment, which augments the difficulty of the event interpretation because of the higher energy and the consequent presence of other reaction products. Moreover, in the decay at rest the relative angle between photons was not measured, but assumed to be equal to  $180^\circ$ . It has to be noticed that Monte Carlo

events were generated in the center of the detector. For real events the effect of some energy leakage through the walls of the detector can appear despite of the fiducial volume cut.

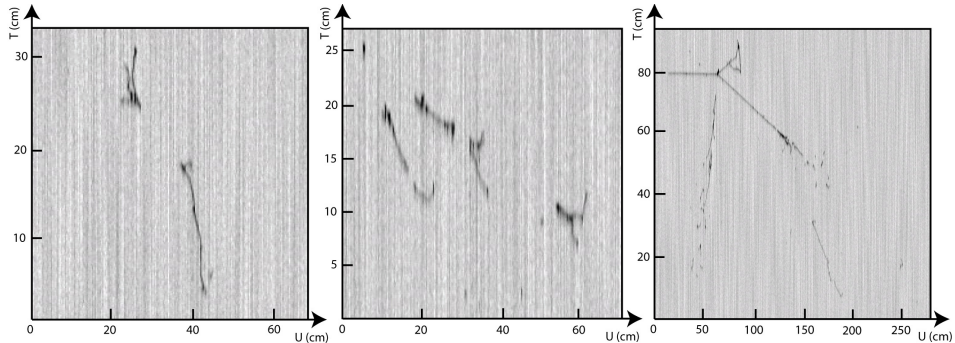


Fig. 14. Examples of simulated neutral pion decays as seen by FLUKA-ICARUS detector: decay at rest (left plot),  $\pi^0$  from  $\Sigma^+$  decay (middle plot) and from  $\pi^-$  interaction in LAr (right plot).

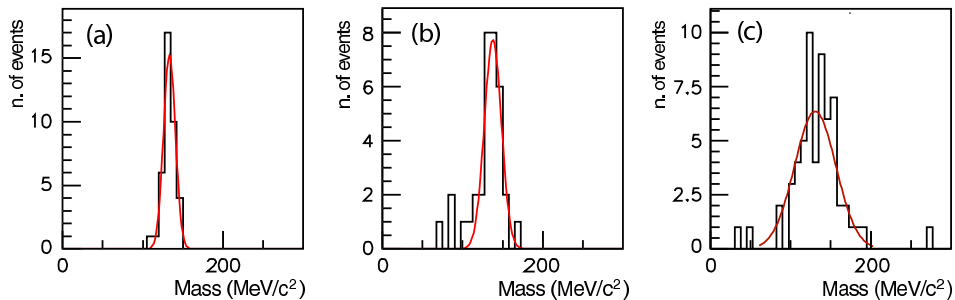


Fig. 15. (a)  $m_{\gamma\gamma}$  for MC simulated pion decays at rest:  $m_{\gamma\gamma} = 133.3 \text{ MeV}/c^2$  (RMS =  $7.4 \text{ MeV}/c^2$ ); (b)  $m_{\gamma\gamma}$  from MC simulated  $\Sigma^+ \rightarrow \pi^0 + p$  decay:  $m_{\gamma\gamma} = 137.8 \text{ MeV}/c^2$  (RMS =  $10.7 \text{ MeV}/c^2$ ); (c)  $m_{\gamma\gamma}$  from MC simulated 2 GeV  $\pi^-$  LAr interactions:  $m_{\gamma\gamma} = 130.6 \text{ MeV}/c^2$  (RMS =  $25.8 \text{ MeV}/c^2$ ).

## 8. Simulation of $\pi^0$ production in $\nu$ interactions

In the previous sections it has been shown that the results of the analysis of real and simulated events with  $\pi^0$  production are consistent. Therefore, the same method of generation, measurement and reconstruction was applied to simulated neutrino-induced pion production to check the potentiality of the LAr technique in this respect. An important point in the future experiments looking for  $\theta_{13}$  is the efficiency of distinction between photon-induced showers from  $\pi^0$  decay and the electron showers from electron neutrino interactions.

The neutral pion production from NC neutrino interactions in the Liquid Argon ICARUS detector was simulated using NUX [12]–FLUKA chain of programs. The neutrino energies were chosen in a region of maximal oscillation probability between 1 and 5 GeV.

The measured distribution of the two photons invariant mass is presented in Fig. 16. To disentangle the proper photon pair combination for events with four and six photons pointing to the same vertex, the pairs with minimum  $\chi^2$  of the difference between measured values of  $(\gamma, \gamma)$  invariant mass and the  $\pi^0$  mass were selected, see Eq. (6). The position of the maximum was found to be consistent with the  $\pi^0$  mass value. The emission of 5  $\eta$  (547) mesons was observed in the generated sample and its mass was properly reproduced. The width of the  $\pi^0$  peak is  $\sigma = 17.8 \pm 1.6$  MeV/ $c^2$  (13.1%). This value is similar to the one obtained for the real data ( $\sigma = 22.6 \pm 2.9$  MeV/ $c^2$ , 16.1%), the difference being probably due to the larger background at the earth surface. The shape of  $m_{\gamma\gamma}$  distribution presents deviations from the Gaussian shape as it was found with the real data.

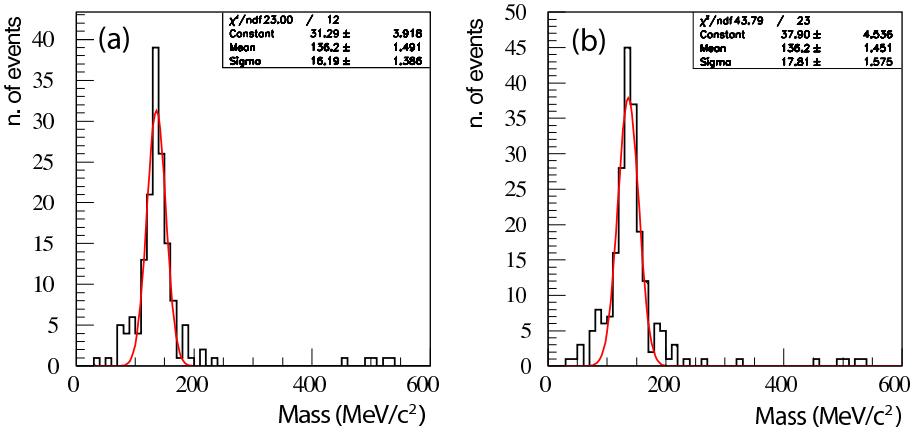


Fig. 16. Two photon invariant mass from Monte Carlo events initiated by muon neutrino NC interactions. Pions from both primary and secondary vertices are included; one pion events (a), all (one and multi-pions) events (b).

After the inspection of Monte Carlo events coming from the tails of the two photons invariant mass distribution it was found that some  $\pi^0$ s were emitted from a secondary neutral vertex close to the primary one. Some of them were the products of  $\Lambda$  or  $K$  meson decays. Wrong assignment of the decay vertex obviously leads to a shift in the reconstructed mass. In the LAr TPC the good spatial resolution allows to distinguish the majority of the secondary vertices if their distance from the main hadronic interaction vertex is larger than about 1 cm. The problem is much more severe in

water or sandwich-like detectors which are characterized by much worse spatial resolution. It should be noted that the expected percentage of the all secondary neutral pions was found to be as large as about 25% at 2 GeV and 43% at 5 GeV in FLUKA based generator.

These results give a hint of the capability of the LAr TPC technique to solve the problem of the electron/ $\pi^0$  identification, despite of the fact that they were almost entirely based on simulation and supported by data only through the width of the  $\pi^0$  mass distribution.

### 8.1. Neutral current (NC) $\nu_\mu$ events as a background to $\nu_e$ CC interactions

An event with  $\pi^0$  production in NC  $\nu_\mu$  interaction can be misidentified with an electron from CC  $\nu_e$  interaction if one of the two following configurations occurs:

- (1) One photon from the decay can be lost when its energy it is too small to allow its distinction in the crowded environment surrounding it ( $E < 20$  MeV); the calculation based on the decay kinematics shows that the percentage of events with such decay photon, being a function of the parent pion energy, never exceeds 2.5%. The showers of energy larger than 20 MeV were always properly recognized in the simulated events.
- (2) The two photon showers overlap: the minimum angle between the two photon showers from the decay is sufficiently large to allow to distinguish the two showers only for a  $\pi^0$  energy up to about 1 GeV. The minimum angle decreases from  $70.1^\circ$  at 100 MeV to  $13.7^\circ$  at 1 GeV. If one does not require a full  $\pi^0$  mass reconstruction as a pion selection tool the shower overlap is less critical. The possible overlapping effect for more energetic pion decays was already studied: it was shown [13] that the  $\frac{dE}{dx}$  method can be efficiently applied, in LAr detector, to distinguish the beginning of the electron track from the beginning of the lepton pair that comes from the photon conversion.

Moreover, internal conversion due to the Dalitz decay (1.2% of cases) or conversion close to the primary vertex (5.5% of cases within the first 1 cm) gives raise to misidentification of a photon shower as an electron induced cascade in the 6.7% of cases. In the most frequently populated interval of  $\pi^0$  energy (200 ÷ 400 MeV), in about 2% of events the low energy photon can be lost. By multiplying this probability by 0.067 it follows that, in our detector, the total probability of the  $\pi^0$  background is expected to be at the level of  $10^{-3}$ .

## 9. Conclusions

A sample of 212 events with at least two photon showers pointing at the apparent interaction vertex were selected from the data collected during the surface test run of the ICARUS detector. Methods of measuring the shower energy and shower direction were developed and the invariant mass of the photon pairs was reconstructed. The position of the maximum in the invariant  $(\gamma, \gamma)$  mass distribution for the 196 real  $\pi^0$  candidates, obtained after a fiducial volume cut, was found to be in agreement with the value of the  $\pi^0$  mass, thus confirming the common assumption that the  $\pi^0$ s are the main source of the photons. The RMS uncertainty of the reconstructed  $\pi^0$  invariant mass was found to be equal to  $36.7 \pm 3.4$  MeV/ $c^2$  (27.3%).

An improved analysis was carried out in order to clean the initial event sample from the events measured in a crowded environment caused by other tracks and interactions surrounding the  $\pi^0$  candidates. As a result, the position of the maximum in the invariant  $(\gamma, \gamma)$  mass for the 97 surviving real  $\pi^0$  candidates was found again to be in agreement with the  $\pi^0$  mass. Moreover, the RMS uncertainty of the reconstructed  $\pi^0$  invariant mass was found to be equal to  $(22.6 \pm 2.9)$  MeV/ $c^2$  (16.1%), which is significantly narrower than the mass distribution for the initial event sample. The  $\pi^0$  mass distribution was in good agreement with the distributions obtained for the Monte Carlo generated events with neutral pion production in hadronic and neutrino interactions. The agreement between the data and the Monte Carlo confirms the validity of the shower energy and shower direction reconstruction methods. It also demonstrates the potential of the ICARUS LAr TPC, because simple quality cuts were sufficient to obtain good results in very difficult conditions of the surface test, detector commissioning and tuning of the electronics.

It was found that in the photon energy range from 50 to 5000 MeV the simulated electromagnetic shower energy resolution  $\sigma(E)/E$  can be approximated by the formula  $\sigma(E)/E = P1/\sqrt{E} + P2$  with the parameters  $P1 = (0.33 \pm 0.03) \sqrt{\text{MeV}}$  and  $P2 = 0.012 \pm 0.002$ .

To simulate the future measurements in the CNGS beam, neutrino interactions at incident energies between 1 and 5 GeV were generated using the FLUKA package. Scanning and measurements of the showers pointing to the primary and secondary vertices were carried out, and the two photon mass was reconstructed for events with different number of showers. It was demonstrated that in most cases a proper reconstruction of up to the three pions coming from the same vertex was possible. A few events with  $\eta(547)$  meson decay into two photons were found in simulated events and properly reconstructed.

The asymmetric decays of  $\pi^0$ s as a background to  $\nu_e$  charge current events were discussed. It was found that it is likely to lose the photon of energy smaller than about 20 MeV but the percentage of events with such a photon never exceeds 2.5%. The frequency of events that could be misidentified with events containing single electron shower, because of the low energy photon lost for either the Dalitz decay or the events with the second photon converting close to the neutrino interaction vertex was estimated to be at the level of one per mil.

In summary: our analysis implies very good prospects for the recognition and energy measurement of electromagnetic showers during the ICARUS running in the Gran Sasso laboratory, where the background due to other signals in the neighborhood of neutrino interactions will be negligible.

We wish to dedicate this work to the memory of our friend and colleague Fulvio Mauri, co-author of the paper, who prematurely passed away on March, 2008. We would like to warmly thank the many technical collaborators that contributed to the construction of the detector and to its operation. We are glad of the financial and technical support of our funding agencies and in particular of the Istituto Nazionale di Fisica Nucleare (INFN). The Polish groups acknowledge the support of the Ministry of Science and Higher Education in Poland, 105,160,620,621/E-344,E-340,E-77,E-78/SPB/ICARUS/P-03/DZ211-214/2003-2008, 1P03B04130 and N N202 0299 33.

## REFERENCES

- [1] C. Rubbia, CERN-EP/77-08 (1977).
- [2] S. Amerio *et al.*, *Nucl. Instrum. Methods* **A527**, 329 (2004).
- [3] F. Arneodo *et al.*, *Nucl. Instrum. Methods* **A508**, 287 (2003).
- [4] S. Amoruso *et al.*, *Nucl. Instrum. Methods*. **A516**, 68 (2004).
- [5] S. Amoruso *et al.*, *Nucl. Instrum. Methods* **A523**, 275 (2004).
- [6] A. Ankowski *et al.*, *Eur. Phys. J.* **C48**, 667 (2006).
- [7] S. Amoruso *et al.*, *Eur. Phys. J.* **C33**, 233 (2004).
- [8] M. Miyajima *et al.*, *Phys. Rev.* **A9**, 1438 (1974).
- [9] S. Amoruso *et al.*, *Nucl. Instrum. Methods* **A523**, 233 (2004).
- [10] W.M. Yao *et al.*, *J. Phys. G* **33**, 1 (2006).
- [11] A. Fassò *et al.*, “The physics models of FLUKA: status and recent developments”, Computing in High Energy and Nuclear Physics 2003 Conference (CHEP2003), La Jolla, CA, USA, March 24–28, 2003 (paper MOMT2005), eConf **C0303241** (2003), hep-ph/0306276.
- [12] A. Rubbia, “NUX — neutrino generator”, 1st Workshop on Neutrino–Nucleus Interactions in the Few GeV Region (NuInt01), Tsukuba, Japan, 13–16 December, 2001.
- [13] D. Stefan, T. Wachała, *Acta Phys. Pol. B* **37**, 2187 (2006).